



# Preparation of One-dimensional Bamboo-like $\text{Cu}_{2-x}\text{S}@C$ Nanorods with Enhanced Lithium Storage Properties



Yunhui Wang<sup>a,1</sup>, Yiyong Zhang<sup>a,1</sup>, He Li<sup>a</sup>, Yueying Peng<sup>a</sup>, Jiyang Li<sup>a</sup>, Jing Wang<sup>a</sup>, Bing-Joe Hwang<sup>b</sup>, Jinbao Zhao<sup>a,\*</sup>

<sup>a</sup> State Key Lab of Physical Chemistry of Solid Surfaces, College of Chemistry and Chemical Engineering, Collaborative Innovation Center of Chemistry for Energy Materials, State-Province Joint Engineering Laboratory of Power Source Technology for New Energy Vehicle, Xiamen University, Xiamen 361005, Fujian, China

<sup>b</sup> NanoElectrochemistry Laboratory, Department of Chemical Engineering, National Taiwan University of Science and Technology, Taipei 106, Taiwan

## ARTICLE INFO

### Article history:

Received 15 May 2017

Received in revised form 30 June 2017

Accepted 4 July 2017

Available online 5 July 2017

### Keywords:

bamboo-like nanorods

cuprous sulfide

carbon coating

electrochemical performances

batteries

## ABSTRACT

Nanostructure construction and surface modification are effective ways to improve the electrochemical performances of electrode materials, especially for the conversion reaction-based materials. In this study, one-dimensional carbon coating bamboo-like  $\text{Cu}_{2-x}\text{S}$  nanorods have been delicately designed in a template-free method. The structure and morphology are well characterized via different instruments such as X-ray diffraction analysis (XRD), scanning electron microscopy (SEM) and transmission electron microscopy (TEM). Tested in lithium batteries as the anode, the  $\text{Cu}_{2-x}\text{S}@C$  electrode shows superior electrochemical performances to pristine  $\text{Cu}_{2-x}\text{S}$ . At 1 and 2 C, the  $\text{Cu}_{2-x}\text{S}@C$  nanorod electrode releases 309 and 277  $\text{mAh g}^{-1}$  after 300 cycles. At high rates of 15 and 22 C, the electrode still exhibits 269 and 264  $\text{mAh g}^{-1}$ . The kinetics of electrodes are also investigated by means of cyclic voltammetry (CV) and galvanostatic intermittence titration (GITT) measurements, proving the enhanced electrochemical properties. Thus, the one-dimensional bamboo-like  $\text{Cu}_{2-x}\text{S}$  voided nanorods can be a promising candidate for high-performance batteries.

© 2017 Elsevier Ltd. All rights reserved.

## 1. Introduction

As an attracting energy storage system, lithium ion batteries (LIBs) have been broadly used in portable devices such as mobile phones, lap-tops and other electronic devices. With the ever-increasing demand on energy consumption, particularly, the electric vehicles and electric grids, higher performances lithium ion batteries are urgently needed [1–3]. As an important component, the electrode materials play a key role in improving performances of LIBs. Great effort has been paid to investigate new-type anode materials instead of traditional graphite-kind materials.  $\text{Li}_4\text{Ti}_5\text{O}_{12}$  has been commercially applied in power batteries as an anode material since it is a zero-strain insertion material with good reversibility, high thermal stability and relative high charge/discharge plateaus avoiding formation of hazardous lithium dendrite. However, its disadvantages such as low specific

capacity ( $175 \text{mAh g}^{-1}$ ), low energy density ( $266 \text{Wh kg}^{-1}$ ) and poor electronic conductivity ( $10^{-13} \text{Scm}^{-1}$ ) hinder its further application in high energy density and high performance storage systems [4–6]. Recently,  $\text{Li}_3\text{VO}_4$  with desirable lithium ion conductivity and higher theoretical specific capacity ( $394 \text{mAh g}^{-1}$ ) has attracted great attention, which also exhibits impressive cyclability [7–9]. However, the environmental-unfriendly and toxic vanadium inhibits it from extensive application. Therefore, continuous and numerous attempts should be paid to explore more suitable alternatives.

Metal sulfides, with high specific capacities and good electronic conductivity, have been drawing more and more attentions [10–15]. Among them, copper sulfides are one of fascinating materials with high theoretical capacities and electrical conductivity [16–20]. Nevertheless, the conversion reaction-based materials suffer from the serious pulverization problem during charge and discharge processes, leading to the loss of active species and rapid capacity fading. To cope with this problem, many strategies have been proposed to improve their cycle performances. Nanostructure construction is an effective method to improve the cycling stability [21–23]. Reducing the material size not only guarantees the short transporting path of lithium ions to achieve

\* Corresponding author.

E-mail address: [jbzhao@xmu.edu.cn](mailto:jbzhao@xmu.edu.cn) (J. Zhao).

<sup>1</sup> Y.H. Wang and Y. Y. Zhang contributed equally to this work and share first authorship.

excellent rate capability, but also validly accommodates the volume expansion during lithium (de) intercalation. In previous studies, one-dimension copper sulfides have successfully prepared [22]. Although this unique one-dimensional nanostructure permits better accommodation of volume change as well as short lithium ion transport path, the detrimental side reactions with electrolytes still exist, deteriorating the performances of batteries [24,25]. Carbon coating is a common and valid way used in various materials to improve the electrochemical performances [26–28]. This strategy is generally adopted in the Li-S batteries to constrict diffusion of sulfur species [29,30], which could become a powerful technique to improve the electrochemical performances of cuprous sulfides.

In this paper, one-dimensional bamboo-like  $\text{Cu}_{2-x}\text{S}@C$  voided nanorods are delicately designed and successfully prepared without using any templates. The one-dimension  $\text{CuS}$  nanorod precursors are first prepared, followed by carbon coating and calcination. The coating carbon acts as a barrier to hinder the loss of active species and improve the electric conductivity. The volume expansion is well accommodated due to the one-dimensional nanorod structure and the numerous voids inside. The carbon coating layer well protect cuprous sulfides from side reactions with electrolytes, greatly boosting the long-life cycling performance. Furthermore, kinetics of electrodes is investigated by different electrochemical measurements, proving the enhanced lithiation properties. Thus, the one-dimensional bamboo-like  $\text{Cu}_{2-x}\text{S}@C$  electrode exhibits the admirable cycle performance and outstanding rate capability.

## 2. Experimental Section

### 2.1. Materials Preparation

All chemicals purchased from Sinopharm Chemical Reagent Co., Ltd were used without any treatment.

#### 2.1.1. Synthesis of $\text{CuS}$ nanorods

$\text{CuS}$  nanorods were synthesized via a previously reported method [22]. Typically, 0.0075 mol  $\text{CuSO}_4 \cdot 5\text{H}_2\text{O}$  were added into 80 mL dimethyl sulfoxide (DMSO) under magnetic stirring for 10 min. The mixture was then transferred to a 100 mL Teflon-sealed autoclave, which was heated at  $180^\circ\text{C}$  for 6 h and then cooled down to room temperature naturally. The precipitates were

filtered and washed by deionized water and ethanol several times followed by drying at  $60^\circ\text{C}$  for 12 h under vacuum.

#### 2.1.2. Preparation of $\text{CuS}@C$ nanorods

0.6 g  $\text{CuS}$  and 1.2 g glucose (Sinopharm Chemical Reagent Co., Ltd) were added to 50 mL deionized water with stirring for 10 min, which was transferred to a 100 mL Teflon-sealed autoclave to be heated at  $190^\circ\text{C}$  for 6 h. The black precipitates were obtained and washed by ethanol and water.

#### 2.1.3. Synthesis of bamboo-like $\text{Cu}_{2-x}\text{S}@C$ nanorods

All the obtained  $\text{CuS}@C$  precursors were put into a porcelain boat. The boat was placed in the middle of a quartz tube, which was heated at  $500^\circ\text{C}$  under Ar flowing gas for 8 h.

#### 2.1.4. Synthesis of bamboo-like $\text{Cu}_{2-x}\text{S}$ nanorods

The  $\text{CuS}$  precursor was put into a porcelain boat, which was calcined under same condition as the those of  $\text{Cu}_{2-x}\text{S}@C$ .

#### 2.1.5. Synthesis of pyrolytic carbon

1.2 g glucose was dissolved into 50 mL deionized water with stirring for a while, which was transferred to a 100 mL Teflon-sealed autoclave to be heated at  $190^\circ\text{C}$  for 6 h. The product was washed several times with deionized water and ethanol followed by drying at  $60^\circ\text{C}$  for 6 h. Then the dried product was calcined under the same condition as those of  $\text{Cu}_{2-x}\text{S}@C$ .

## 2.2. Structure Characterization

The microstructures and morphologies were characterized by X-ray diffraction (XRD, Rigagu/mini Flex 600) with  $\text{Cu K}\alpha$  radiation, scanning electron microscope (SEM, Hitachi S-4800) and transmission electron microscope (TEM, Tecnai F30). The specific surface area was measured by the Brunauer-Emmett-Teller (BET) method using  $\text{N}_2$  adsorption and desorption isotherms (Micrometrics ASAP 2020). The content of carbon was ascertained by the element analysis (Vario EL III).

## 2.3. Cell Fabrication and Electrochemical Characterization

To prepare the working electrodes, the slurry (mixtures of 70 wt% as-prepared  $\text{Cu}_{2-x}\text{S}@C$  nanorods, 15 wt% acetylene black and 15 wt% polyvinylidene difluoride, all dispersed in the N-methyl-2-

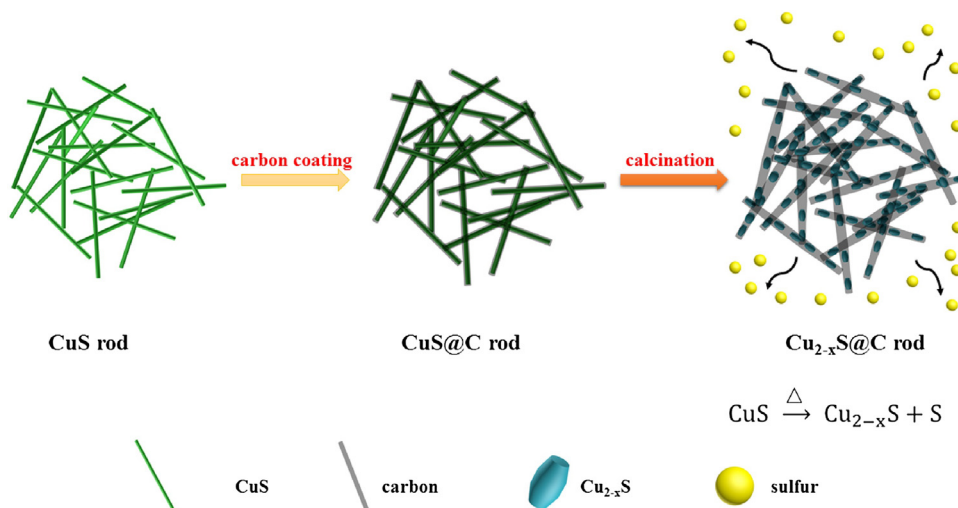


Fig. 1. Synthetic scheme of bamboo-like  $\text{Cu}_{2-x}\text{S}@C$  nanorods.

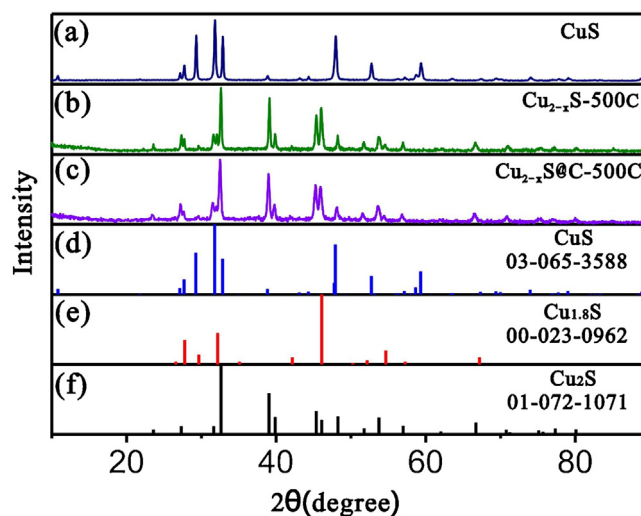


Fig. 2. XRD patterns of (a) CuS, (b)  $\text{Cu}_{2-x}\text{S}$ , (c)  $\text{Cu}_{2-x}\text{S}@C$  and corresponding standard cards of (d) CuS, (e)  $\text{Cu}_{1.8}\text{S}$  and (f)  $\text{Cu}_2\text{S}$ .

pyrrolidinone solvent) was coated on a copper foil current collector using doctor blade and dried at  $60^\circ\text{C}$  overnight under vacuum. The electrolyte was consisted of 1 M LiTFSI salt (J&K Chemical) in the mixed solvent of 1, 3-dioxolane and dimethyl ether (DOL/DME, 1:1 volume ratio, Aladin). The 2016-type coin cells were assembled in an argon-filled glove box. Lithium foil and the Celgard 2400 were used as the counter electrode and the separator, respectively. Galvanostatic charge/discharge measurements were performed from 1.0 to 3.0 V at different C rates ( $1\text{ C} = 337\text{ mA g}^{-1}$ ) on the Neware CT-3008W Battery Cycler (Shenzhen, China). The electrochemical impedance spectra (EIS) were tested in the frequency of  $10^{-1}$  to  $10^{-5}$  Hz on the Solartron Modulab 1287/1260. The cyclic voltammetry (CV) test was conducted on the CHI-1030C electrochemical work station (Shanghai, China) at the scanning of  $0.2\text{ mV s}^{-1}$  between 1.0 and 3.0 V. The assembly of  $\text{Cu}_{2-x}\text{S}$  and pyrolytic carbon electrodes and electrochemical tests are the same as the  $\text{Cu}_{2-x}\text{S}@C$  electrode. The mass loading ( $\text{Cu}_{2-x}\text{S}@C$ ) of electrodes ranged from 1.5 to  $2.0\text{ mg cm}^{-2}$ . The specific capacity was calculated based on the mass of  $\text{Cu}_{2-x}\text{S}$ . For the apparent chemical diffusion coefficient of lithium ion, CV tests with different scan rates ranging from 0.2 to  $1.0\text{ mV s}^{-1}$  and galvanostatic intermittence titration measurements (GITT) were applied to the cells recycled 20 cycles. For the GITT, the cell was discharged/

charged at 0.1 C for 10 min, followed by a relaxation procedure under open circuit for 1 h.

### 3. Results and Discussion

The synthetic scheme is shown in Fig. 1. CuS nanorods are firstly prepared, followed by carbon coating with glucose as the carbon source [22,31]. Then the CuS@C precursor is calcined at  $500^\circ\text{C}$  at the Ar atmosphere. At high temperature, CuS thermally decomposes to  $\text{Cu}_{2-x}\text{S}$  and S [32]. The sublimated elemental S diffuses out and is carried away by loading gas, leaving voids inside the carbon coated nanorods as well as creating the bamboo-like structure. Thus, one-dimensional bamboo-like  $\text{Cu}_{2-x}\text{S}@C$  nanorods are successfully prepared. The crystal nature was characterized by XRD as shown in Fig. 2. The diffraction peaks of synthetic CuS (Fig. 2a) correspond well with the standard card of CuS (JCPDS No. 03-065-3588). After carbon coating, new peaks evolve (Fig. S1a). The peak at  $46^\circ$  is ascribed to  $\text{Cu}_{1.8}\text{S}$  (JCPDS No. 00-023-0962). It was reported that at the high temperature and the high pressure, the reducing ability of glucose could be promoted [33], leading to partially reduction of CuS to  $\text{Cu}_{1.8}\text{S}$ . After calcination, the diffraction pattern is totally different from those of CuS@C (Fig. 2c), whose peaks are well indexed to cuprous sulfides

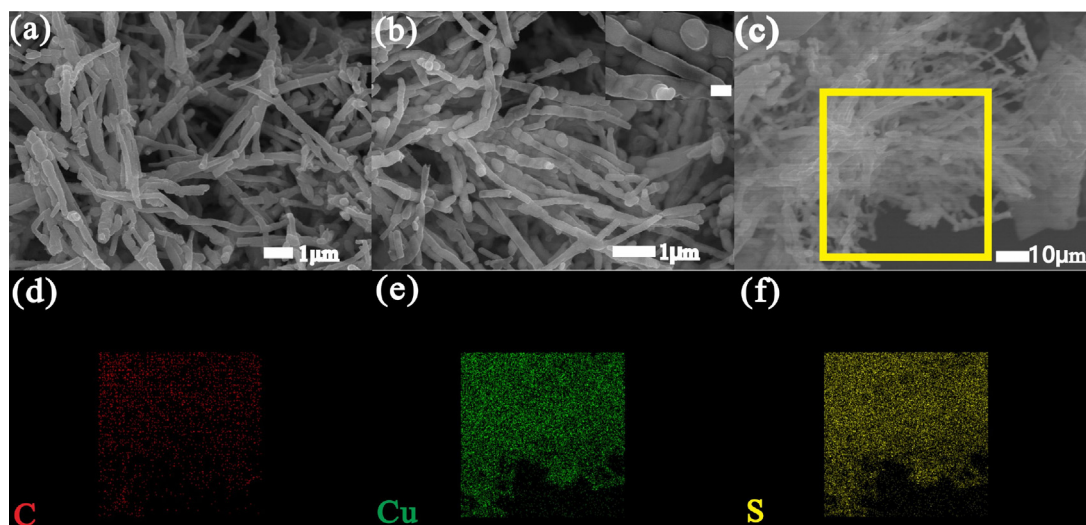
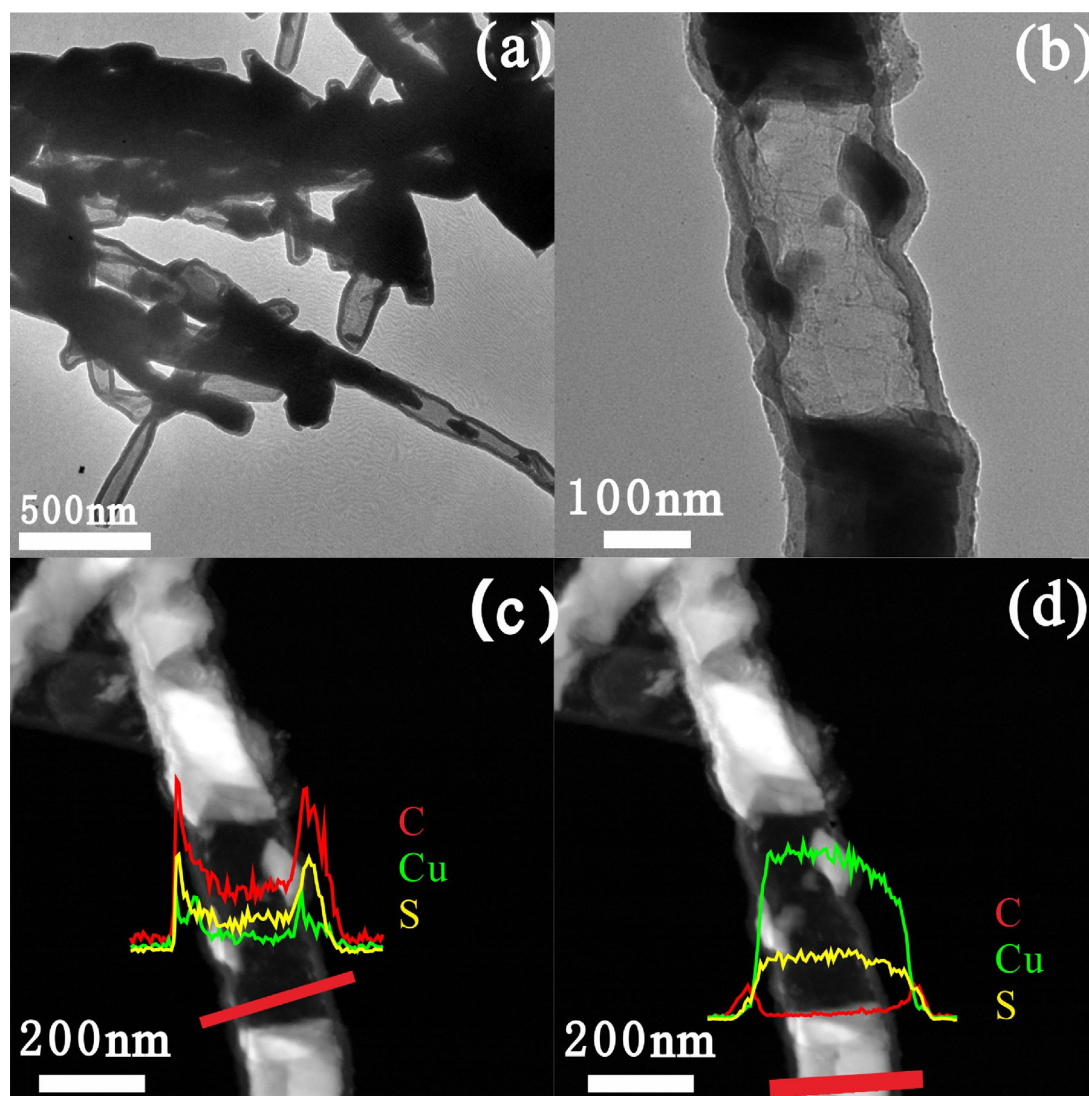


Fig. 3. SEM images of (a) CuS, (b, c)  $\text{Cu}_{2-x}\text{S}@C$  (the scale bar of the inset is 200 nm) and elemental mapping of (d) C, (e) Cu, (f) S.

( $\text{Cu}_2\text{S}$ , JCPDS No. 01-072-1071,  $\text{Cu}_{1.8}\text{S}$ , JCPDS No. 00-023-0962). At high temperature,  $\text{CuS}$  would thermally decompose to cuprous sulfides ( $\text{Cu}_{1.8}\text{S}$  and  $\text{Cu}_2\text{S}$ ) and elemental sulfur [32]. Besides, peaks indexed to carbon could not be seen, indicating the carbon calcined at  $500^\circ\text{C}$  is amorphous.  $\text{CuS}$  nanorods without any coating are also calcined under the same condition (designated as  $\text{Cu}_{2-x}\text{S}$ ). The diffraction peaks are almost the same as those of  $\text{Cu}_{2-x}\text{S}@C$  as shown in Fig. 2b.

SEM images of  $\text{CuS}$  and  $\text{Cu}_{2-x}\text{S}@C$  are shown in Fig. 3. The synthetic  $\text{CuS}$  exhibits a rod-like shape with a smooth surface, diameter of about 200 nm and length of several micrometers. After carbon coating, the morphology is kept well (Fig. S2a). Calcined at  $500^\circ\text{C}$ , the rods grow in sections with knots between each other like the bamboo (Fig. 3b). Voids inside some rods can be clearly observed from the inset. We speculate that the voids are formed as soon as the elemental sulfur was carried off by the flowing gas. In our experiments, we have found that residual yellow substance (supposed to be the elemental sulfur) adhering to the outlet of the quartz tube can be found after annealing. The SEM image (Fig. S2b) of  $\text{Cu}_{2-x}\text{S}$  shows that some bamboo-like rods also appear while some rods without any voids agglomerate. EDX elemental mapping images in selected area show existence of elemental carbon, copper and sulfur, which all distribute homogeneously. To know

more about the microstructure of  $\text{Cu}_{2-x}\text{S}@C$ , the TEM was conducted and Fig. 4a clearly shows that parts of rods are hollow. The high-resolution TEM (HRTEM) (Fig. 4b) shows that the nanorod is wrapped by a uniform layer with thickness of roughly 20 nm. HAADF-STEM and line scanning analysis are used to analyze two regions (hollow and solid regions). Observed from the signal of the hollow region (Fig. 4c), it can be known that the layer mainly contains C, Cu and S also adhere to the wall of the rod, while the middle part of the rod barely includes element Cu and S. On the other side, the signal of the solid region (Fig. 4d) shows that the middle part of the rod is mainly consisted of Cu and S, while the layer is mainly composed of C. The signal intensity of Cu and S is close to 2: 1, which is consistent with the stoichiometry of cuprous sulfide.  $\text{N}_2$  adsorption/desorption analysis was implemented to obtain the specific surface area (SSA) of  $\text{Cu}_{2-x}\text{S}$  and  $\text{Cu}_{2-x}\text{S}@C$ , as shown in Fig. S3. The SSA of  $\text{Cu}_{2-x}\text{S}$  and  $\text{Cu}_{2-x}\text{S}@C$  are 21.2 and  $47.4\text{ m}^2\text{ g}^{-1}$ . The larger SSA of  $\text{Cu}_{2-x}\text{S}@C$  can be ascribed to the bamboo-like hollow structure, where the voids existed inside coated rods contribute more surface area. From above results, it can be confirmed that the  $\text{Cu}_{2-x}\text{S}$  nanorods are wrapped by uniform coating carbon with thickness of about 20 nm, and voids also exist inside the rods. Element analysis was applied to analyze the carbon content of  $\text{Cu}_{2-x}\text{S}@C$ , showing that the content of carbon is 15.8%.



**Fig. 4.** TEM images of (a)  $\text{Cu}_{2-x}\text{S}@C$ , (b) the magnified one and (c, d) HAADF-STEM images and compositional line profiles of C (red), Cu (green), S (yellow) in different areas. (For interpretation of the references to colour in this figure legend, the reader is referred to the web version of this article.)

To test and compare the electrochemical performances of  $\text{Cu}_{2-x}\text{S}$  and  $\text{Cu}_{2-x}\text{S}@C$ , the 2016 type coin cells were assembled with lithium foils as anodes. Both CV curves are shown in Fig. 5a and b. In the first reducing scanning, the  $\text{Cu}_{2-x}\text{S}$  electrode exhibits a small cathodic peak at 2.1 V and a broad, strong cathodic peak at 1.6 V. The former cathodic peak relates to the reduction of  $\text{CuS}$  to  $\text{Cu}_2\text{S}$  and the other correlates to the continuous reduction of  $\text{Cu}_2\text{S}$  to form  $\text{Li}_2\text{S}$  and metal  $\text{Cu}$  [22,34,35]. During the oxidizing scanning, two anodic peaks at 1.9 V and 2.3 V appear. The peak at 1.9 V is relevant to the oxidation of metal  $\text{Cu}$  to  $\text{Cu}^+$  while the electrochemical reaction mechanism of the peak at 2.3 V is intriguing and not fully understood. We speculate that it is related with the over potential caused by activation of  $\text{Li}_2\text{S}$  in the first charging process [16,36]. In the following cycles, the curves of

oxidation are obviously different from those of the initial cycle, which indicates the complicate electrochemical reaction mechanism in this process. However, after 100 cycles, a pair of redox peaks are left, demonstrating that the electrochemical reaction is much more reversible and is also the typical electrochemical behavior of cuprous sulfides [16,37]. The CV curves (Fig. 5b) of  $\text{Cu}_{2-x}\text{S}@C$  are similar with those of  $\text{Cu}_{2-x}\text{S}$ . The main difference is that the intensity of redox peaks is stronger in the case of  $\text{Cu}_{2-x}\text{S}@C$  after 100 cycle, implicating the better cycling reversibility. Fig. 5c and d show the charge-discharge curves in different cycles at 1 C (1 C =  $337 \text{ mA g}^{-1}$ , the calculation of specific capacity is based on the mass of  $\text{Cu}_{2-x}\text{S}$  for both cases.). The initial discharge capacities of  $\text{Cu}_{2-x}\text{S}$  and  $\text{Cu}_{2-x}\text{S}@C$  are 335 and 408  $\text{mAh g}^{-1}$  (the capacity of  $\text{Cu}_{2-x}\text{S}@C$  is calculated based on the mass ratio of  $\text{Cu}_{2-x}\text{S}$ , 84.2%),

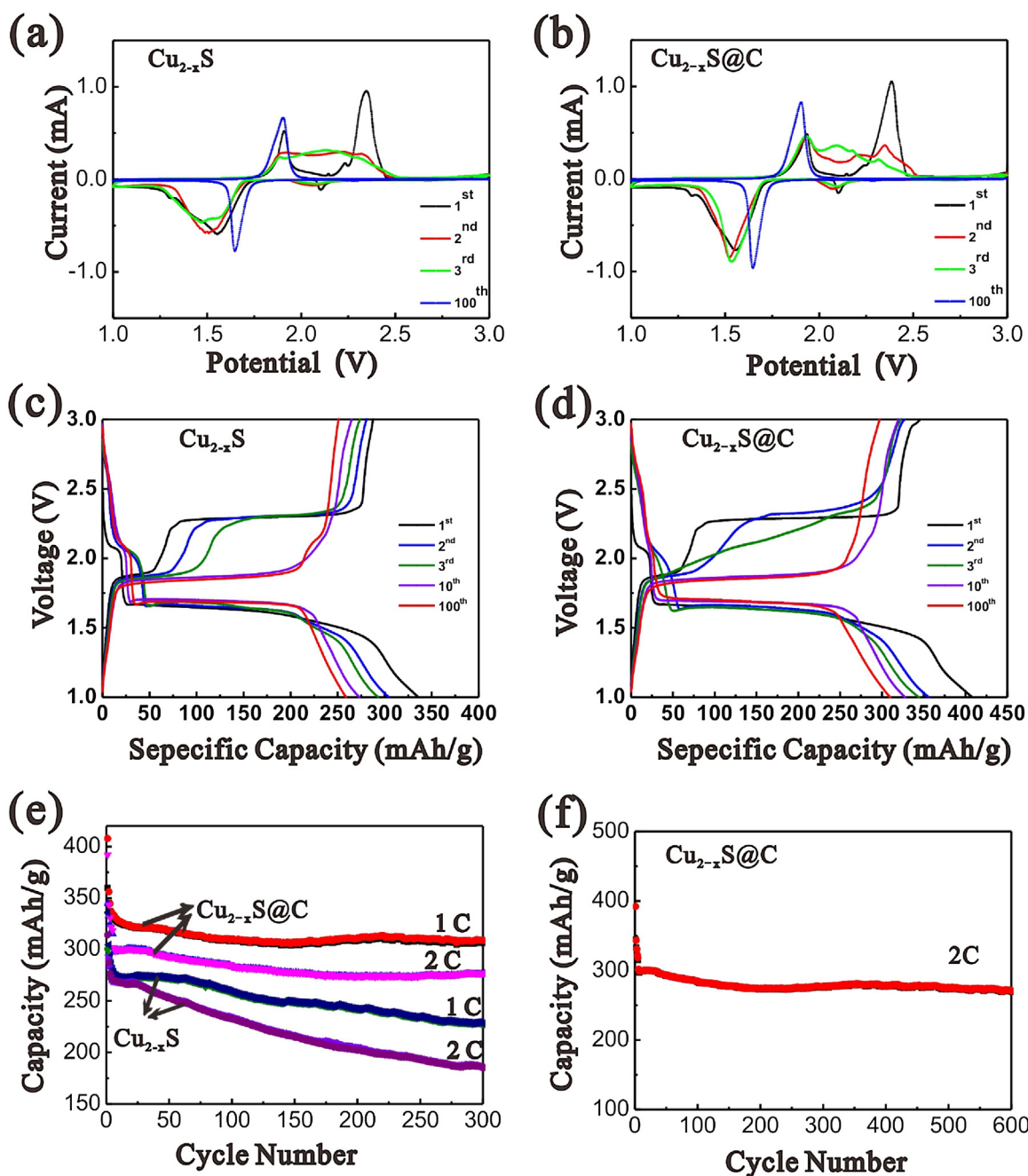


**Fig. 5.** Cyclic voltammetry profiles of (a)  $\text{Cu}_{2-x}\text{S}$  and (b)  $\text{Cu}_{2-x}\text{S}@C$ , charge-discharge curves of (c)  $\text{Cu}_{2-x}\text{S}$  and (d)  $\text{Cu}_{2-x}\text{S}@C$ , (e) cycle performances of both materials at 1 C and 2 C and (f) the long-term cycling test of  $\text{Cu}_{2-x}\text{S}@C$  at 2 C. The calculation of specific capacity is based on the mass of  $\text{Cu}_{2-x}\text{S}$  for both cases.

**Table 1**  
Comparison of cycling performances.

	Current density (mA g <sup>-1</sup> )	Cycles	Reversible capacity (mAh g <sup>-1</sup> )	
Cu <sub>2</sub> S	337	100	270	[18]
C@Cu <sub>1.96</sub> S nanosheet	50	50	240	[48]
Cu <sub>2</sub> S@SWCNT	100	200	260	[34]
Cu <sub>2</sub> S/C	100	100	300	[49]
Cu <sub>2</sub> S/C	337	300	276	[50]
Bamboo-like Cu <sub>2-x</sub> S@C nanorod	337	300	309	this work
	674	600	270	

corresponding coulombic efficiencies are 89.4% and 88.2%, respectively. It is noted that the Cu<sub>2-x</sub>S@C electrode exhibits more initial discharge capacity, even exceeds the theoretical capacity (337 mAh g<sup>-1</sup>) of Cu<sub>2</sub>S. This can be related with the pseudocapacity-like storage behavior of lithium ions on the surface of carbonaceous materials and interaction with oxygen-containing functional groups [38,39]. To verify the speculation, a contrast experiment with the pyrolytic carbon as the active material is conducted. The synthetic procedure can be seen in the experiment section. The cycling test of pyrolytic carbon (Fig. S4) shows that it would release capacities of 68, 34 and 20 mAh g<sup>-1</sup>, respectively, in the first three cycles. Due to the extra capacity contributed by the carbon layer, the initial discharge capacity of Cu<sub>2-x</sub>S@C may exceed the theoretical capacity of Cu<sub>2-x</sub>S@C and the initial coulombic efficiency will be lowered. After 30 cycles, the capacity levels off (about 10 mAh g<sup>-1</sup>), which barely contributes extra capacity.

Cycling performances were conducted to evaluate Cu<sub>2-x</sub>S and Cu<sub>2-x</sub>S@C electrodes at different rates, as seen in Fig. 5e. For the Cu<sub>2-x</sub>S, the capacity drops slowly before 100 cycles, then fades significantly after that. After 300 cycles, reversible capacities of 228 and 186 mAh g<sup>-1</sup> are obtained at 1 C and 2 C, the corresponding capacity retention ratios are 67.9% and 59.2%, respectively. On the contrary, the Cu<sub>2-x</sub>S@C electrode displays superior cyclability. After 300 cycles, the electrodes still release 309 and 277 mAh g<sup>-1</sup>, corresponding capacity retention ratios are 75.8% and 70.7%, respectively. To further show the improved cycling performance, the long-life cycling measurement (Fig. 5f) was implemented to the Cu<sub>2-x</sub>S@C electrode at 2 C. The releasing capacity levels off after 150 cycles. After 600 cycles, it can still release more than 270 mAh g<sup>-1</sup>. Comparison of cycling performances with other reports is shown in Table 1. From those it can be known that the bamboo-like Cu<sub>2-x</sub>S@C nanorods exhibit impressive long-life cycling performances, attributing to the synergistic effect of carbon coating and hollow structure. The side reactions between cuprous sulfides and electrolytes can be inhibited by the coating layer, and the volume expansion during (de)lithiation is well alleviated by the hollow structure. Likewise, it is reported that the peapod-like MnO@C core-shell composite also exhibits impressive cycling stability in long term cycling, which is attributed to the well accommodation of volume expansion by the internal void space, protection by the carbon shell and the spatially confined stable SEI formation [28].

The rate performances of Cu<sub>2-x</sub>S and Cu<sub>2-x</sub>S@C electrodes are shown in Fig. 6. The charge/discharge profiles of both electrodes are nearly the same when the rate is lower than 8 C. When the rate is continually increasing, the plateau gap of Cu<sub>2-x</sub>S electrode enlarges (Fig. 6a), especially at 22 C, indicating the large polarization of the Cu<sub>2-x</sub>S electrode. In contrast, the voltage plateaus have not changed much regardless of the increasing rates (Fig. 6b), demonstrating the lower polarization. Fig. 6c shows that the Cu<sub>2-x</sub>S electrode exhibits 282, 271, 265, 257, 246 and 232 mAh g<sup>-1</sup> at 1, 2, 4, 8, 15 and 22 C, respectively. For the Cu<sub>2-x</sub>S@C electrode, it releases 316, 303, 291, 278, 269 and 264 mAh g<sup>-1</sup>,

when the rate is restored to 1 C, it will regain the capacity of 318 mAh g<sup>-1</sup>. Another obvious difference between them is that when the Cu<sub>2-x</sub>S electrode cycled at high rates (15 and 22 C), the overcharge phenomenon would appear, which is a shortcoming in cuprous sulfides [22]. Coated by the carbon layer, that problem can be solved and the coulombic efficiencies is close to 100% at high rates.

Electrochemical impedance spectra of Cu<sub>2-x</sub>S and Cu<sub>2-x</sub>S@C electrodes in different cycles are shown in Fig. 6e and f. The spectra were analyzed with the equivalent circuit model shown in Fig. S5, where R<sub>s</sub> and R<sub>ct</sub> indicate the impedance of the electrolytes and the charge transfer resistance, CPE and W<sub>o</sub> represent the capacitance of the electrical double layer and the ion diffusion, respectively [40–42]. From the EIS data, a typical profile is consisted of a depressed semicircle at the high frequency and an inclined line at the middle frequency, among which the former one is associated with the charge transfer resistance (R<sub>ct</sub>) and the latter one is correlated with the long-range lithium ion diffusion (W<sub>o</sub>) [43,44]. The fitting parameters of both electrodes are shown in Table 2. After 200 cycles, the R<sub>ct</sub> of the Cu<sub>2-x</sub>S@C electrode is 23.56 Ω, which is smaller than that (58.58 Ω) of Cu<sub>2-x</sub>S, indicating that the carbon layer actually improves the interfacial properties of Cu<sub>2-x</sub>S material. To investigate the difference of the electrode kinetics, CV tests at different scan rates and GITT were implemented after 20 cycles. For both cases, the gap between redox peaks becomes larger with the increasing scan rates (Fig. 7a and c). However, the reductions peaks of Cu<sub>2-x</sub>S shift more negatively than those of Cu<sub>2-x</sub>S@C, indicating the larger polarization and slower electrode kinetics. From Fig. 7b and d, a linear relationship exists between redox peak currents and the square root of scan rates. The Li<sup>+</sup> diffusion coefficients (D) is calculated based on the Randles-Sevcik Eq. (1) [45,46]:

$$i_p = 0.4463nFAC \left( \frac{nFvD}{RT} \right)^{\frac{1}{2}} \quad (1)$$

**Table 2**  
Impedance Parameters of Cu<sub>2-x</sub>S and Cu<sub>2-x</sub>S@1.6C Electrodes

Cu <sub>2-x</sub> S				
	R <sub>s</sub> (Ω)	Error (%)	R <sub>ct</sub> (Ω)	Error (%)
Before cycling	1.854	4.145	227.8	0.8528
50th cycle	2.874	1.774	10.43	1.005
100th cycle	2.917	1.939	9.862	1.045
200th cycle	3.303	2.504	58.58	1.805
Cu <sub>2-x</sub> S@C				
	R <sub>s</sub> (Ω)	Error (%)	R <sub>ct</sub> (Ω)	Error (%)
Before cycling	3.063	1.653	254.5	0.5613
50th cycle	2.695	1.291	12.80	1.371
100th cycle	3.011	1.485	11.39	0.8804
200th cycle	2.722	0.8625	23.56	0.2848

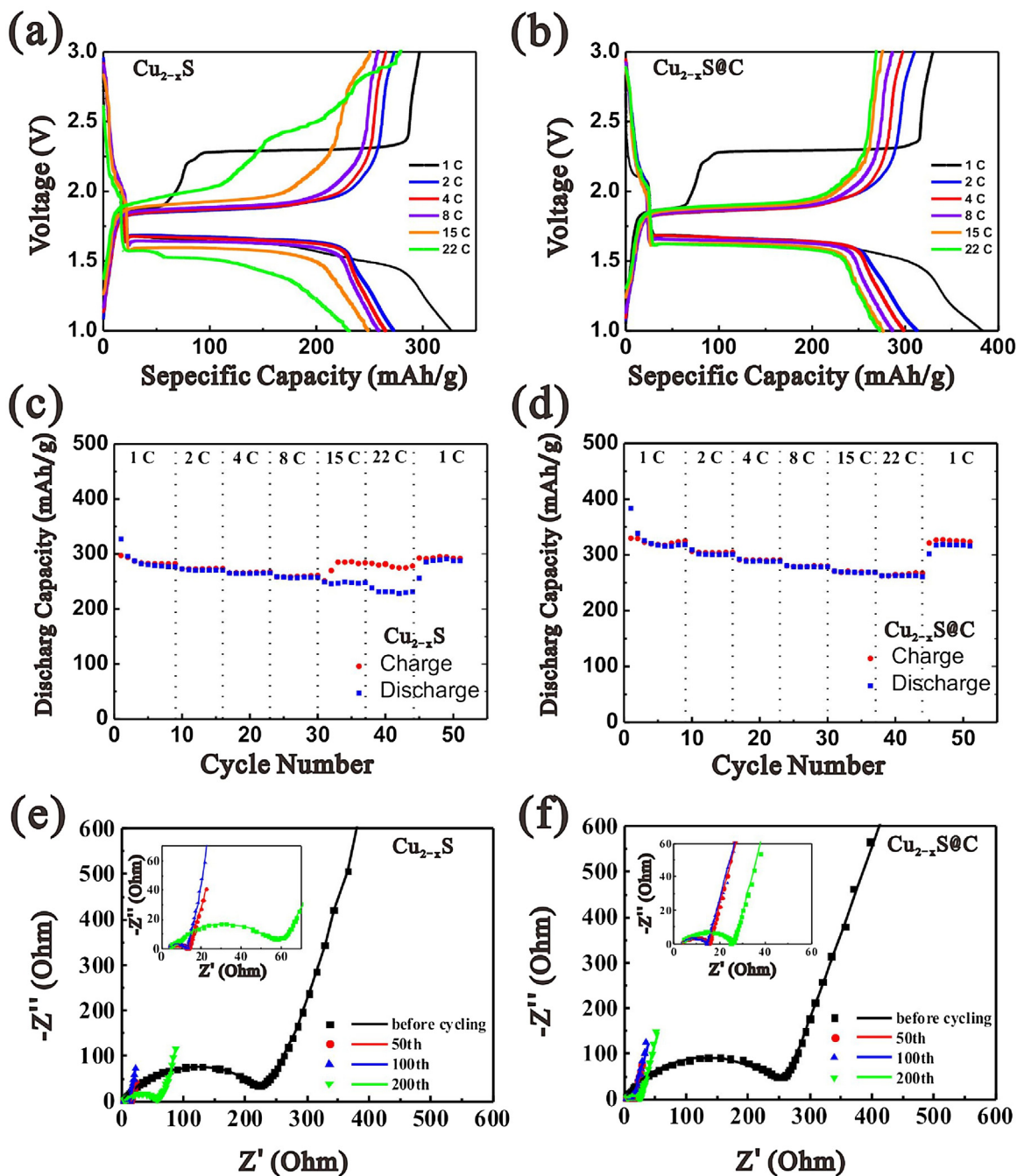


**Fig. 6.** Rate performances and charge/discharge curves of (a, c)  $\text{Cu}_{2-x}\text{S}$  and (b, d)  $\text{Cu}_{2-x}\text{S}@C$ . Electrochemical impedance spectra of (e)  $\text{Cu}_{2-x}\text{S}$  and (f)  $\text{Cu}_{2-x}\text{S}@C$  in different cycles.

where the  $i_p$  is the redox peak current,  $n$  indicates the number of transferred electrons,  $F$  represents the Faraday Constant,  $A$  is the working electrode area,  $C$  stands for the concentration of lithium ion,  $v$  is the scan rate,  $T$  is the temperature,  $R$  is the gas constant and  $D$  stands for the diffusion coefficient. For the  $\text{Cu}_{2-x}\text{S}$ , the calculated  $D$  of oxidation peak ( $P_1$ ) and reduction peak ( $P_2$ ) are  $1.61 \times 10^{-10}$  and  $0.706 \times 10^{-10} \text{ cm}^2 \text{ s}^{-1}$ . The  $D$  of  $P_1$  and  $P_2$  are  $1.72 \times 10^{-10}$  and  $2.59 \times 10^{-10} \text{ cm}^2 \text{ s}^{-1}$  for the  $\text{Cu}_{2-x}\text{S}@C$ , demonstrating the enhanced lithium ion diffusion compared with the pristine one, especially in the reduction (insertion of lithium ion) process.

To get deeper insight the reduction (discharge) process, GITT measurements are performed after 20 cycles, as shown in Fig. 7e. Assuming the lithium ion transport satisfy the Fick's second law,

the  $\text{Li}^+$  diffusion coefficients can be calculated by Eq. (2) [46,47]:

$$D = \frac{4}{\pi\tau} \left[ \left( \frac{m_B V_m}{A M_B} \right) \frac{\Delta E_s}{\Delta E_t} \right]^2, \quad \left( \tau \ll \frac{L^2}{D} \right) \quad (2)$$

where  $D$  stands for the chemical diffusion coefficient of lithium ion,  $\tau$  is the constant current titration time,  $m_B$  and  $M_B$  are the weight and molecular weight of active materials,  $V_m$  is the molar volume of active materials,  $A$  represents the electrode surface area,  $\Delta E_s$  and  $\Delta E_t$  are the steady-state voltage change after a current disturbance and voltage change during the constant current titration,  $L$  is the diffusion length. According to Eq. (2),  $\text{Li}^+$  diffusion coefficients of both electrodes are obtained (Fig. 7f). The  $D$  of  $\text{Cu}_{2-x}\text{S}$  ranges from  $8.72 \times 10^{-10}$  to  $2.29 \times 10^{-15} \text{ cm}^2 \text{ s}^{-1}$ , whereas those of

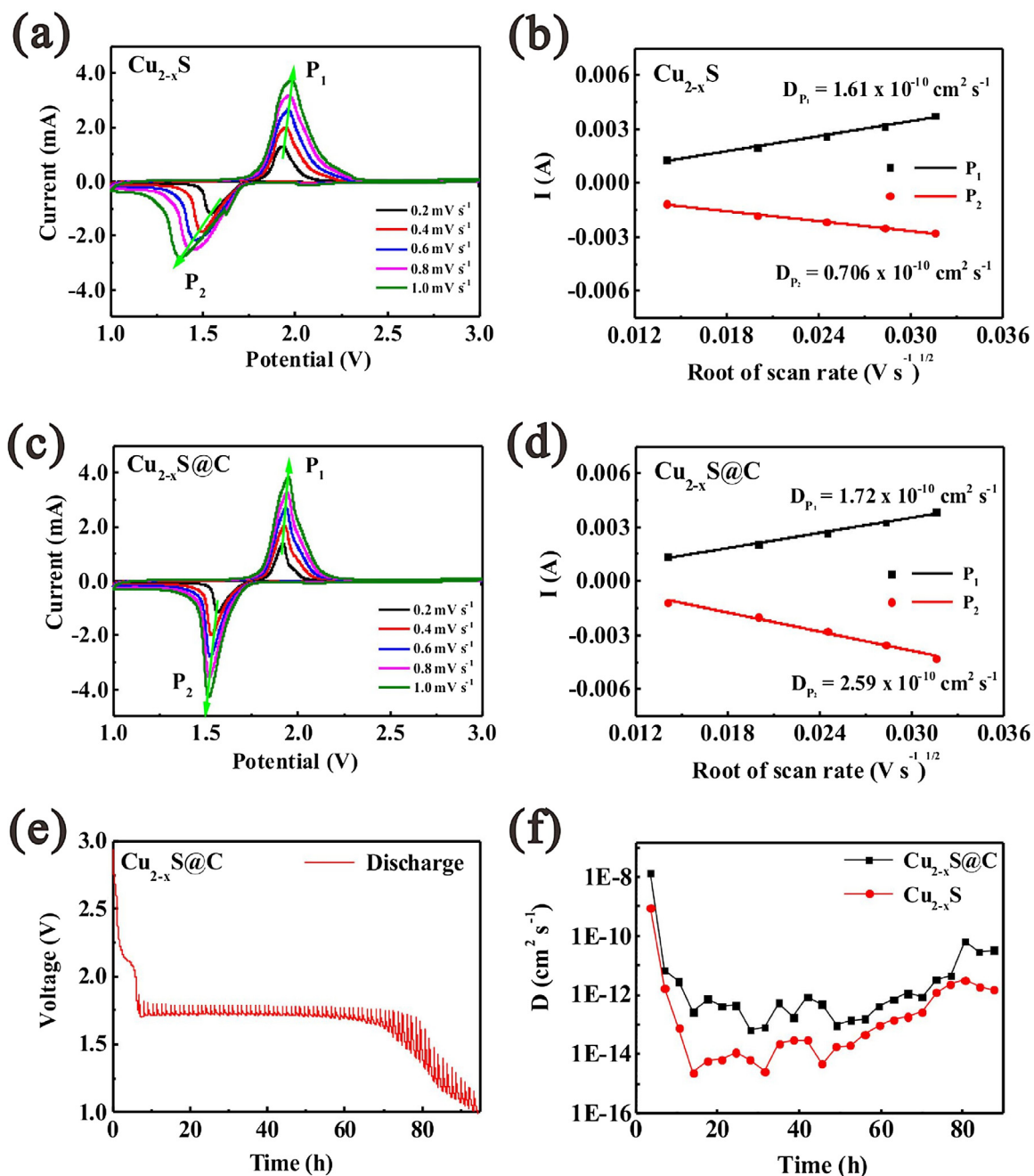


**Fig. 7.** CV profiles of (a)  $\text{Cu}_{2-x}\text{S}$  and (c)  $\text{Cu}_{2-x}\text{S}@C$  at different scan rates between 0.2 and  $1.0 \text{ mV s}^{-1}$  after 20 cycles, relationship between the redox peak current and the square root of the scan rates of (b)  $\text{Cu}_{2-x}\text{S}$  and (d)  $\text{Cu}_{2-x}\text{S}@C$ , (e) the GITT curve of  $\text{Cu}_{2-x}\text{S}@C$  and (f) the calculated  $\text{Li}^+$  chemical diffusion coefficient of  $\text{Cu}_{2-x}\text{S}$  and  $\text{Cu}_{2-x}\text{S}@C$  after 20 cycles.

$\text{Cu}_{2-x}\text{S}@C$  are between  $1.36 \times 10^{-8}$  and  $9.62 \times 10^{-14} \text{ cm}^2 \text{ s}^{-1}$ . Correspond to the CV results, the lithium ion diffusion of  $\text{Cu}_{2-x}\text{S}@C$  in the discharge process is much faster than that of  $\text{Cu}_{2-x}\text{S}$ , which can be attributed to the carbon coating layer and the voids inside the rods [26]. In our previous study, we have proved that complexing with carbonaceous materials is beneficial to improve the ion diffusion in the cuprous sulfide [20]. The  $D$  of  $\text{Cu}_{2-x}\text{S}@C$  nanorods are higher than those of  $\text{CuS}/\text{graphene}$  composite previously reported, which can be ascribed to the one-dimensional nanorod structure and more integrated carbon coating.

Taken above results into account, we conclude that the carbon layer has made a great difference to the electrochemical performances of  $\text{Cu}_{2-x}\text{S}$ , which the function is summed up as follow: 1) reduce the side reactions between active materials and

electrolytes, 2) validly inhibit active material from loss during long term cycling [29], 3) to serve as an elastic shell to accommodate the volume change during charge and discharge processes [26,29]. The bamboo-like structure with voids also makes a contribution to the outstanding electrochemical performances: 1) better accommodate the volume expansion to enhance the structure stability, 2) a relatively short lithium ion diffusion pathway to improve the rate performance.

#### 4. Conclusion

Bamboo-like  $\text{Cu}_{2-x}\text{S}@C$  nanorods have successfully prepared without using any templates. Combining both the coating carbon layer and the unique bamboo-like nanorod structure, the  $\text{Cu}_{2-x}\text{S}@C$

shows outstanding cycle performance and superior rate capability. At the high rate of 2 C, it can still release 270 mAhg<sup>-1</sup> with the capacity retention of 68.9% after 600 cycles. When cycling at rates of 15 and 22 C, the Cu<sub>2-x</sub>S@C electrode still exhibits 269 and 264 mAhg<sup>-1</sup>, respectively, with nearly 100% coulombic efficiency, showing better electrochemical performances than its counterpart. Considering all advantages mentioned above, the bamboo-like Cu<sub>2-x</sub>S@C nanorod material may become promising anode candidates for high performance LIBs.

## Acknowledgements

The authors gratefully acknowledge the financial support of National Natural Science Foundation of China (Grant No. 21273185 and No. 21321062) and sincerely thank Profs. Daiwei Liao for the valuable suggestions.

## Appendix A. Supplementary data

Supplementary data associated with this article can be found, in the online version, at <http://dx.doi.org/10.1016/j.electacta.2017.07.022>.

## References

- [1] N.S. Choi, Z. Chen, S.A. Freunberger, X. Ji, Y.K. Sun, K. Amine, G. Yushin, L.F. Nazar, J. Cho, P.G. Bruce, Challenges facing lithium batteries and electrical double-layer capacitors, *Angew. Chem. Int. Ed. Engl.* 51 (2012) 9994–10024.
- [2] J.W. Choi, D. Aurbach, Promise and reality of post-lithium-ion batteries with high energy densities, *Nat. Rev. Mater.* 1 (2016) 16013.
- [3] G. Zhu, K. Wen, W. Lv, X. Zhou, Y. Liang, F. Yang, Z. Chen, M. Zou, J. Li, Y. Zhang, W. He, Materials insights into low-temperature performances of lithium-ion batteries, *J. Power Sources* 300 (2015) 29–40.
- [4] L. Yu, H.B. Wu, X.W. Lou, Mesoporous Li<sub>4</sub>Ti<sub>5</sub>O<sub>12</sub> hollow spheres with enhanced lithium storage capability, *Adv. Mater.* 25 (2013) 2296–2300.
- [5] J. Liu, K. Song, P.A. van Aken, J. Maier, Y. Yu, Self-supported Li<sub>4</sub>Ti<sub>5</sub>O<sub>12</sub>-C nanotube arrays as high-rate and long-life anode materials for flexible Li-ion batteries, *Nano Lett.* 14 (2014) 2597–2603.
- [6] T. Yuan, Z. Tan, C. Ma, J. Yang, Z.-F. Ma, S. Zheng, Challenges of Spinel Li<sub>4</sub>Ti<sub>5</sub>O<sub>12</sub> for Lithium-Ion Battery Industrial Applications, *Adv. Energy Mater.* (2017) 1601625.
- [7] Y. Shi, J.Z. Wang, S.L. Chou, D. Wexler, H.J. Li, K. Ozawa, H.K. Liu, Y.P. Wu, Hollow structured Li<sub>3</sub>VO<sub>4</sub> wrapped with graphene nanosheets in situ prepared by a one-pot template-free method as an anode for lithium-ion batteries, *Nano Lett.* 13 (2013) 4715–4720.
- [8] Y. Yang, J. Li, X. He, J. Wang, D. Sun, J. Zhao, A facile spray drying route for mesoporous Li<sub>3</sub>VO<sub>4</sub>/C hollow spheres as an anode for long life lithium ion batteries, *J. Mater. Chem. A* 4 (2016) 7165–7168.
- [9] W. Zhang, J. Luo, X. Li, J. Liang, Y. Zhu, Y. Qian, Facile synthesis and electrochemistry of a new cubic rocksalt Li<sub>x</sub>V<sub>y</sub>O<sub>2</sub> (x = 0.78, y = 0.75) electrode material, *J. Mater. Chem. A* 5 (2017) 5148–5155.
- [10] Z. Wang, X. Li, Y. Yang, Y. Cui, H. Pan, Z. Wang, B. Chen, G. Qian, Highly dispersed β-NiS nanoparticles in porous carbon matrices by a template metal-organic framework method for lithium-ion cathode, *J. Mater. Chem. A* 2 (2014) 7912–7916.
- [11] J. He, Y. Chen, W. Lv, K. Wen, C. Xu, W. Zhang, Y. Li, W. Qin, W. He, From Metal-Organic Framework to Li<sub>2</sub>S@C-Co-N Nanoporous Architecture: A High-Capacity Cathode for Lithium-Sulfur Batteries, *ACS Nano* 10 (2016) 10981–10987.
- [12] H.H. Fan, H.H. Li, K.C. Huang, C.Y. Fan, X.Y. Zhang, X.L. Wu, J.P. Zhang, Metastable Marcasite-FeS<sub>2</sub> as a New Anode Material for Lithium Ion Batteries: CNFs-Improved Lithiation/Delithiation Reversibility and Li-Storage Properties, *ACS Appl. Mater. Interfaces* 9 (2017) 10708–10716.
- [13] Z.Y. Li, A. Ottmann, T. Zhang, Q. Sun, H.P. Meyer, Y. Vaynzof, J.H. Xiang, R. Klingeler, Preparation of hierarchical C@MoS<sub>2</sub>@C sandwiched hollow spheres for lithium ion batteries, *J. Mater. Chem. A* 5 (2017) 3987–3994.
- [14] Y.H. Wang, B.H. Wu, X.Y. He, Y.Y. Zhang, H. Li, Y.Y. Peng, J. Wang, J.B. Zhao, Synthesis of Micro/nanostructured Co<sub>9</sub>S<sub>8</sub> Cubes and Spheres as High Performance Anodes for Lithium Ion Batteries, *Electrochim. Acta* 230 (2017) 299–307.
- [15] J. He, P. Li, W. Lv, K. Wen, Y. Chen, W. Zhang, Y. Li, W. Qin, W. He, Three-dimensional hierarchically structured aerogels constructed with layered MoS<sub>2</sub>/graphene nanosheets as free-standing anodes for high-performance lithium ion batteries, *Electrochim. Acta* 215 (2016) 12–18.
- [16] X. Wang, Y. Wang, X. Li, B. Liu, J. Zhao, A facile synthesis of copper sulfides composite with lithium-storage properties, *J. Power Sources* 281 (2015) 185–191.
- [17] C. Feng, L. Zhang, Z. Wang, X. Song, K. Sun, F. Wu, G. Liu, Synthesis of copper sulfide nanowire bundles in a mixed solvent as a cathode material for lithium-ion batteries, *J. Power Sources* 269 (2014) 550–555.
- [18] G. Kalimuldina, I. Taniguchi, High performance stoichiometric Cu<sub>2</sub>S cathode on carbon fiber current collector for lithium batteries, *Electrochim. Acta* 224 (2017) 329–336.
- [19] M. Zhou, N. Peng, Z. Liu, Y. Xi, H. He, Y. Xia, Z. Liu, S. Okada, Synthesis of sub-10 nm copper sulphide rods as high-performance anode for long-cycle life Li-ion batteries, *J. Power Sources* 306 (2016) 408–412.
- [20] H. Li, Y. Wang, J. Huang, Y. Zhang, J. Zhao, Microwave-assisted Synthesis of CuS/Graphene Composite for Enhanced Lithium Storage Properties, *Electrochim. Acta* 225 (2017) 443–451.
- [21] R. Cai, J. Chen, J. Zhu, C. Xu, W. Zhang, C. Zhang, W. Shi, H. Tan, D. Yang, H.H. Hng, T.M. Lim, Q. Yan, Synthesis of Cu<sub>2</sub>S/Cu Nanotubes and Their Lithium Storage Properties, *J. Phys. Chem. C* 116 (2012) 12468–12474.
- [22] X. Li, X. He, C. Shi, B. Liu, Y. Zhang, S. Wu, Z. Zhu, J. Zhao, Synthesis of One-Dimensional Copper Sulfide Nanorods as High-Performance Anode in Lithium Ion Batteries, *ChemSusChem* 7 (2014) 3328–3333.
- [23] G. Chen, L. Yan, H. Luo, S. Guo, Nanoscale Engineering of Heterostructured Anode Materials for Boosting Lithium-Ion Storage, *Adv. Mater.* 28 (2016) 7580–7602.
- [24] J. Gao, M.A. Lowe, Y. Kiya, H.D. Abruña, Effects of Liquid Electrolytes on the Charge/Discharge Performance of Rechargeable Lithium/Sulfur Batteries: Electrochemical and in-Situ X-ray Absorption Spectroscopic Studies, *J. Phys. Chem. C* 115 (2011) 25132–25137.
- [25] J. Cabana, L. Monconduit, D. Larcher, M.R. Palacin, Beyond intercalation-based Li-ion batteries: the state of the art and challenges of electrode materials reacting through conversion reactions, *Adv. Mater.* 22 (2010) E170–E192.
- [26] H. Li, H. Zhou, Enhancing the performances of Li-ion batteries by carbon-coating: present and future, *Chem. Commun.* 48 (2012) 1201–1217.
- [27] C.H. Xu, B.H. Xu, Y. Gu, Z.G. Xiong, J. Sun, X.S. Zhao, Graphene-based electrodes for electrochemical energy storage, *Energy Environ. Sci.* 6 (2013) 1388–1414.
- [28] S. Wang, Y. Xing, C. Xiao, H. Xu, S. Zhang, A peapod-inspired MnO@C core-shell design for lithium ion batteries, *J. Power Sources* 307 (2016) 11–16.
- [29] Y. Hwa, J. Zhao, E.J. Cairns, Lithium Sulfide (Li<sub>2</sub>S)/Graphene Oxide Nanospheres with Conformal Carbon Coating as a High-Rate, Long-Life Cathode for Li/S Cells, *Nano Lett.* 15 (2015) 3479–3486.
- [30] X. Liang, C. Hart, Q. Pang, A. Garsuch, T. Weiss, L.F. Nazar, A highly efficient polysulfide mediator for lithium-sulfur batteries, *Nat. Commun.* 6 (2015) 5682.
- [31] X.W. Lou, J.S. Chen, P. Chen, L.A. Archer, One-Pot Synthesis of Carbon-Coated SnO<sub>2</sub> Nanocolloids with Improved Reversible Lithium Storage Properties, *Chem. Mater.* 21 (2009) 2868–2874.
- [32] E. Godočíková, P. Baláž, J.M. Criado, C. Real, E. Gock, Thermal behaviour of mechanochemically synthesized nanocrystalline CuS, *Thermochim. Acta* 440 (2006) 19–22.
- [33] J.F. Shen, B. Yan, M. Shi, H.W. Ma, N. Li, M.X. Ye, One step hydrothermal synthesis of TiO<sub>2</sub>-reduced graphene oxide sheets, *J. Mater. Chem.* 21 (2011) 3415–3421.
- [34] X. Meng, S.C. Riba, J.A. Libera, Q. Wu, H.-H. Wang, A.B.F. Martinson, J.W. Elam, Tunable core-shell single-walled carbon nanotube-Cu<sub>2</sub>S networked nanocomposites as high-performance cathodes for lithium-ion batteries, *J. Power Sources* 280 (2015) 621–629.
- [35] A. Débart, L. Dupont, R. Patrice, J.M. Tarascon, Reactivity of transition metal (Co, Ni, Cu) sulphides versus lithium: The intriguing case of the copper sulphide, *Solid State Sci.* 8 (2006) 640–651.
- [36] Y. Yang, G. Zheng, S. Misra, J. Nelson, M.F. Toney, Y. Cui, High-capacity micrometer-sized Li<sub>2</sub>S particles as cathode materials for advanced rechargeable lithium-ion batteries, *J. Am. Chem. Soc.* 134 (2012) 15387–15394.
- [37] B. Jache, B. Mogwitz, F. Klein, P. Adelhelm, Copper sulfides for rechargeable lithium batteries: Linking cycling stability to electrolyte composition, *J. Power Sources* 247 (2014) 703–711.
- [38] Y. Lv, B. Chen, N. Zhao, C. Shi, C. He, J. Li, E. Liu, Interfacial effect on the electrochemical properties of the layered graphene/metal sulfide composites as anode materials for Li-ion batteries, *Surf. Sci.* 651 (2016) 10–15.
- [39] H.S. Oktaviano, K. Waki, Understanding the Li Storage Sites in MWCNTs: SEI, the Key for Delithiation at High Potential, *J. Electrochem. Soc.* 163 (2015) A442–A446.
- [40] Z. Deng, Z. Zhang, Y. Lai, J. Liu, J. Li, Y. Liu, Electrochemical Impedance Spectroscopy Study of a Lithium/Sulfur Battery: Modeling and Analysis of Capacity Fading, *J. Electrochem. Soc.* 160 (2013) A553–A558.
- [41] H. Chen, C. Wang, Y. Dai, S. Qiu, J. Yang, W. Lu, L. Chen, Rational Design of Cathode Structure for High Rate Performance Lithium-Sulfur Batteries, *Nano Lett.* 15 (2015) 5443–5448.
- [42] J. Song, Z. Yu, T. Xu, S. Chen, H. Sohn, M. Regula, D. Wang, Flexible freestanding sandwich-structured sulfur cathode with superior performance for lithium? sulfur batteries, *J. Mater. Chem. A* 2 (2014) 8623–8627.
- [43] X. Li, H. Lin, W. Cui, Q. Xiao, J. Zhao, Fast Solution-Combustion Synthesis of Nitrogen-Modified Li<sub>4</sub>Ti<sub>5</sub>O<sub>12</sub> Nanomaterials with Improved Electrochemical Performance, *ACS Appl. Mater. Interfaces* 6 (2014) 7895–7901.
- [44] N. Schweikert, H. Hahn, S. Indris, Cycling behaviour of Li/Li<sub>4</sub>Ti<sub>5</sub>O<sub>12</sub> cells studied by electrochemical impedance spectroscopy, *Physical Chemistry Chemical Physics* 13 (2011) 6234–6240.
- [45] Y. Chen, J.-M. Tarascon, C. Guery, Exploring sulfur solubility in ionic liquids for the electrodeposition of sulfide films with their electrochemical reactivity toward lithium, *Electrochim. Acta* 99 (2013) 46–53.
- [46] Y. You, H.R. Yao, S. Xin, Y.X. Yin, T.T. Zuo, C.P. Yang, Y.G. Guo, Y. Cui, L.J. Wan, J.B. Goodenough, Subzero-Temperature Cathode for a Sodium-Ion Battery, *Adv. Mater.* 28 (2016) 7243–7248.

- [47] P. Liu, J.J. Vajo, J.S. Wang, W. Li, J. Liu, Thermodynamics and Kinetics of the Li/FeF<sub>3</sub> Reaction by Electrochemical Analysis, *J. Phys. Chem. C* 116 (2012) 6467–6473.
- [48] Z. Zhang, Y. An, J. Feng, L. Ci, B. Duan, W. Huang, C. Dong, S. Xiong, Carbon coated copper sulfides nanosheets synthesized via directly sulfurizing Metal-Organic Frameworks for lithium batteries, *Mater. Lett.* 181 (2016) 340–344.
- [49] Y. Liu, B. Jin, Y.F. Zhu, X.Z. Ma, X.Y. Lang, Synthesis of Cu<sub>2</sub>S/carbon composites with improved lithium storage performance, *Int. J. Hydrogen Energy* 40 (2015) 670–674.
- [50] F. Han, W. Li, D. Li, A. Lu, In Situ Electrochemical Generation of Mesostructured Cu<sub>2</sub>S/C Composite for Enhanced Lithium Storage: Mechanism and Material Properties, *ChemElectroChem* 1 (2014) 733–740.